

A numerical assessment of wall shear stress changes after endovascular stenting

F. Nicoud^{a,*}, H. Vernhet^b, M. Dazat^b

^aUniversity Montpellier II-CNRS UMR 5149, CC 051, 34095 Montpellier Cedex 5, France

^bUniversity Montpellier I - Laboratory of Cardiovascular Physiology EA 2992, France

Accepted 10 September 2004

Abstract

This theoretical/numerical study aims at assessing the haemodynamic changes induced by endovascular stenting. By using the classical one-dimensional linear pressure waves theory in elastic vessels, we first show that the modulus of the reflection coefficient induced by an endovascular prosthesis is most likely small since it is proportional to the stent-to-wavelength ratio. As a direct consequence, the wall motion of the elastic (stented) artery can be prescribed a priori and the coupled fluid–structure problem does not have to be solved for assessing the haemodynamic changes due to stenting. Several 2D axisymmetric calculations are performed to solve the unsteady incompressible Navier–Stokes equations on moving meshes for different types of (stented) arteries. The numerical results suggest that endovascular stenting increases the systo-diastolic variations of the wall shear stress (by 35% at the middle of the stent, by almost 50% in the proximal transition region). Additional calculations show that over-dilated stents produce less haemodynamic perturbations. Indeed, the increase of the amplitude of the wall shear stress variations over the cardiac cycle is only 10% when the stent radius is equal to the radius of the elastic artery at systole (instead of being equal to the mean artery radius). © 2004 Elsevier Ltd. All rights reserved.

Keywords: Stenting; Restenosis; Wall shear stress; Compliance; Numerical method

1. Motivation and objectives

Angioplasty with or without endovascular stenting is an established minimally invasive technique that is used as treatment of occlusive disease in medium to large arteries. It has been applied extensively in the coronary, renal, and peripheral vascular systems. The use of intravascular stents tends to lower the complication rate although restenosis rates as high as 15–30% after 6 months have been observed in human coronary arteries (Rau et al., 1998; Serruys et al., 2002). Coated stents eluting antimitotic agents such as sirolimus and paclitaxel inhibit intimal proliferation. Preliminary reports have showed extremely low rates of restenosis over the short and mid-term

(Morice et al., 2002; Grube et al., 2003). However, considering the long-standing changes in wall mechanics induced by stent placement, long-term results of coated stents are still required. Besides, a better understanding of the mechanical effects induced by stenting could lead to improved prosthesis with lower failure rates and smaller coating requirements (if any). This study is a contribution to this quest for better stent design.

One possible explanation for the trend in restenosis relies on the haemodynamic modifications induced by the prosthesis. Changes in wall shear stress (WSS) induce endothelial dysfunction (Caro et al., 1969), ultimately leading to intimal hyperplasia and restenosis. Davies et al. (2001) suggest that the magnitude of the shear stress is of secondary importance to the spatial and temporal fluctuations of this quantity. In vivo testing performed by Rolland et al. (1999) and Vernhet et al. (2000, 2001) show that endovascular stenting

*Corresponding author. Tel.: +33 4 67 14 48 46;
fax: +33 4 67 14 93 16.

E-mail address: nicoud@math.univ-montp2.fr (F. Nicoud).

induces a large modification of arterial compliance and thus may modify the propagation of arterial waves by introducing additional reflections. The first objective of this study is then to assess the amount of pressure wave reflection due to stenting (Section 2). Another expected effect of the compliance mismatch induced by stenting is to modify the details of blood motion in the stented area. Specifically, the time-averaged (over the cardiac cycle) WSS might be changed, as well as the level of its systo-diastolic variations. The second goal of this paper is to clarify the amount of changes in blood motion that can be expected in relation to endovascular stenting (Section 3). Previous studies have addressed the effects of stenting at a micro-scale level, including the geometrical description of the struts shape and spacing (Berry et al., 2000; Bénard et al., 2003). These studies provide information relevant to the haemodynamic changes immediately after stenting, before the wires have been integrated with the surrounding tissue. For example, the numerical results obtained by Berry et al. (2000) suggest that the flow may reattach downstream of the wires when the strut spacing is greater than about six wire diameters. On the contrary, the present study is dealing with the global effects of the compliance mismatch, neglecting the details of the prosthesis structure. Instead of considering a rigid wall with a micro-scale geometrical description of the struts shape (Berry et al., 2000; Bénard et al., 2003), we model the prosthesis as a uniform elastic tube with its own compliance. The results of this study are more relevant to long-standing stenting, after the wires have been integrated with the surrounding tissue. The reason for considering this point of view is that intimal hyperplasia is certainly a long lasting phenomenon compared to the integration of the stent wires by the vessel: for example, only one week after stenting, Robinson et al. (1988) observed a nearly continuous endothelial and pseudo-endothelial cell layer on the luminal surface of the stented rabbit aorta while intimal hyperplasia is only completed after 6–12 weeks for this model. Therefore, a micro-scale analysis of the blood flow changes including the struts details is only relevant to acute stenting effects. In this paper we consider a complementary point of view in order to provide relevant information about the long-standing haemodynamic effects of stenting.

2. Pressure waves reflection due to stenting

2.1. Basic equations

The general one-dimensional equations describing the pulsatile blood flow in compliant arteries are well known since the work of Hughes and Lubliner (1973). They describe the evolution of u and P , the averaged (over the cross section of the artery) velocity and relative pressure,

respectively. Following Reuderink et al. (1989), the non-linear terms are often neglected. Furthermore, considering a segment whose cross-section area (A) and compliance ($A' = dA/dP$) do not depend on the space variable x and letting $P = \hat{P} \exp(-j\omega t)$ and $u = \hat{u} \exp(-j\omega t)$, where $j^2 = -1$ and ω is the wave pulsation, the following Helmholtz equation can be derived from the classical linear wave equation:

$$d^2 \hat{P}/dx^2 + k^2 \hat{P} = 0. \quad (2.1)$$

The complex wave number is $k = \sqrt{\omega(\rho\omega + jf_v)A'/A}$, where ρ stands for the blood density and f_v is related to the viscous drag and can be derived from the Womersley velocity profile (Womersley, 1955). The complex wave speed is $c = \omega/k$ and the general solution within a homogeneous segment is

$$\begin{aligned} \hat{P} &= P^+ e^{jk(x-x_0)} + P^- e^{-jk(x-x_0)}, \\ \hat{u} &= \frac{k}{\rho\omega + jf_v} (P^+ e^{jk(x-x_0)} - P^- e^{-jk(x-x_0)}), \end{aligned} \quad (2.2)$$

where x_0 is the axial position of the left boundary of the segment and P^+ and P^- correspond to the amplitude of the forward and backward pressure waves. Their values are determined in order to satisfy the boundary conditions at $x = x_0$ and $x = x_0 + L$ where L is the length of the segment.

2.2. Modelling the endovascular stenting

For the purpose of modelling the wave reflection induced by an endovascular stent placed in an elastic artery, three successive homogeneous segments are considered, each having its own set of constant area and compliance (see Fig. 1). Each physical quantity in segment number i ($i = 1, 2, 3$) is denoted with indice i . Conservation of the total flow rate and energy at the interfaces 1–2 and 2–3 requires, for $j = 1, 2$:

$$\begin{aligned} A_j \hat{u}_j(x_{0_j} + L_j) &= A_{j+1} \hat{u}_{j+1}(x_{0_{j+1}}), \\ \hat{P}_j(x_{0_j} + L_j) &= \hat{P}_{j+1}(x_{0_{j+1}}). \end{aligned} \quad (2.3)$$

Two boundary conditions at $x = x_{0_1} = 0$ and $x = x_{0_3} + L_3$ are needed in order to close the problem. In order to focus on the stent response, non-reflecting boundary conditions are prescribed at both sides, leading to

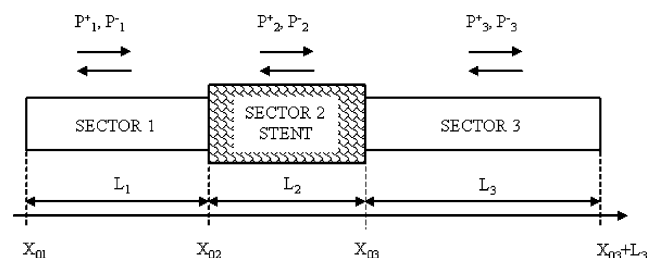


Fig. 1. Schematic of the three homogeneous segments used to build a model of stented artery as regards propagation and reflexion.

$P_1^+ = 1$ and $P_3^- = 0$. The four remaining wave amplitudes, viz. $P_2^+, P_3^+, P_1^-, P_2^-$, are determined by solving Eqs. (2.3) for $j = 1, 2$. The complex coefficient of wave reflection due to the stent is then defined as $R_{\text{stent}} = \exp(-2jk_1L_1)P_1^-/P_1^+$. After some algebra one finds out that

$$R_{\text{stent}} = \frac{A_2K_2(A_1K_1 - A_3K_3) \cos(k_2L_2) - j(A_1K_1A_3K_3 - (A_2K_2)^2) \sin(k_2L_2)}{A_2K_2(A_1K_1 + A_3K_3) \cos(k_2L_2) - j(A_1K_1A_3K_3 + (A_2K_2)^2) \sin(k_2L_2)}, \quad (2.4)$$

where $K_i = k_i/(\rho\omega + jf_{v_i})$. This theoretical result will serve as a support of the wall motion used in the numerical study.

3. Wall shear stress changes due to stenting

The simple 1D analysis provided in Section 2 cannot be used to gain insights about the details of the fluid motion modifications related to artery stenting. Indeed, no reasonable assumption regarding the shape of the velocity profile within the transition area can be formulated a priori and the multi-dimensional Navier–Stokes equations must be solved (assuming Newtonian blood rheology). The solver used in this study is based on the projection method of Chorin (1967) with finite-element discretization and Arbitrary Lagrangian Eulerian formulation to handle moving boundaries. This code has been extensively validated by computing classical (Medic and Mohammadi, 1999) as well as blood flow specific test cases (Nicoud, 2002).

3.1. Computational domain

Since our objective is to investigate the global effect of the compliance mismatch induced by stenting, the endovascular prosthesis is modelled as a uniform duct (the details of the struts are not represented) whose wall is not compliant. Such “prosthesis” is inserted within an elastic artery with compliant wall, as depicted in Fig. 2. The computational domain is sufficiently short to assume constant host artery characteristics and neglect the viscous damping of waves. The flow rate entering the domain is taken as $Q(x_{\text{inlet}}, t) = Q_0 + Q_1 \exp(j\omega(t - x_{\text{inlet}}/c))$, where ω is the pulsation, x_{inlet} is the axial

position of the inlet section and Q_0 and Q_1 stand for the steady and pulsed parts of the flow rate. The mechanical and geometrical data were obtained from animal experimentations performed by Vernhet et al. (2001): the pulsation is $\omega = 8\pi$, the mean artery radius is $R_0 = 1.5$ mm, the distensibility coefficient of the non-

stented artery is $A'/A = 20,7 \times 10^{-6} \text{ Pa}^{-1}$ and the length of the stent is $L_{\text{stent}} = 13$ mm. After stenting, acute measurements (Vernhet et al., 2001) show that the compliance at the stent level is approximately three times smaller than in the non-stented vessel. Measurements made three months later (Vernhet et al., 2003) show that long-standing stenting is also responsible for increased compliance values upstream from the stent, resulting in a larger compliance ratio of order 5–6. In any case, the compliance at the stent level is several times smaller than that of the host vessel and has been neglected during this numerical study (rigid prosthesis assumption). Note, however, that there would be no fundamental issues in accounting for the wall motion at the stent level.

Actually, the motion of the vessel boundary results from the coupling between the fluid and wall mechanics and the local radius is mostly related to the pressure field. Such a coupling is difficult to handle since the density of blood and tissues are of the same order and because the rheology of the vessels is far from well understood. Under the linear elasticity assumption, Tortoriello and Pedrizzetti (2004) recently used a perturbative approach in order to replace the coupled fluid–vessel problem by a cascade of two simpler weakly coupled problems. In this approach, the first problem provides the exact solution into a rigid vessel, the second one approximates the blood flow modifications due to the compliant wall. Since the WSS is expected to be very sensitive to the wall motion, we did follow a different approach where the exact fluid flow equations (and not their truncated linear expansion) are solved for. Since we are mostly interested in the response of the fluid mechanics to wall motion perturbations, the fluid–wall coupling problem can be avoided by prescribing the wall motion a priori. In the absence of reflection and in the case of an elastic uniform artery whose mean radius is R_0 , the wall motion induced by a propagative pressure wave of pulsation ω may be written as

$$R(x, t) = R_0(1 + \varepsilon e^{j(\omega t - kx)}), \quad k = \frac{\omega}{c}, \quad (3.1)$$

where the wave number k is related to the speed of the (forward) pressure wave c . Note that $\varepsilon = \max(R(x, t) - R_0)/R_0$, the relative amplitude of the radius variations,

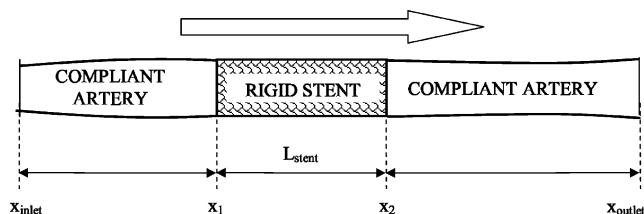


Fig. 2. Schematic of the computational domain.

is a small parameter of the problem: it is zero for a perfectly rigid artery while the animal experiments of Vernhet et al. (2001) suggest $\varepsilon \simeq 0.05$. The speed of propagation is fixed by stating that the non-stented artery being uniform along the streamwise direction, the mass flow rate at any section $x = X$ should be the time-lagged version of the mass flow rate at $x = x_{\text{inlet}}$. The conservation of mass applied to the artery sector $x_{\text{inlet}} < x < X$ then implies that (Nicoud, 2002)

$$c = \frac{Q_1}{2A_0\varepsilon} + O(1), \quad A_0 = \pi R_0^2, \quad (3.2)$$

where $O(1)$ is a term of order unity which can be neglected since c is of order $1/\varepsilon$ according to Eq. (3.2). From the physiological data obtained by Vernhet et al. (2001), the following values were used for the flow rate: $Q_0 \simeq 2413 \text{ mm}^3/\text{s}$ and $Q_1 \simeq 1761 \text{ mm}^3/\text{s}$. Eq. (3.2) then leads to $c \simeq 2492 \text{ mm/s}$. With $\omega = 8\pi$, the corresponding wavelength is $\lambda \simeq 623 \text{ mm}$. In the case where the vessel is stented between x_1 and x_2 (see Fig. 2), the wall displacement is virtually zeroed (fully rigid stent) for $x_1 < x < x_2$ and the following expression is valid for any axial position and time :

$$R(x, t) = R_0(1 + \varepsilon f(x)e^{j(\omega t - kx)}) + (1 - f(x))\delta R_{\text{stent}}, \quad (3.3)$$

where the damping function is $f(x) = [1 - \tanh(x - x_1)]/2$ for $x < (x_1 + x_2)/2$ and $f(x) = [1 + \tanh(x - x_2)]\exp(jk(x_2 - x_1))/2$ for $x > (x_1 + x_2)/2$ and $\delta R_{\text{stent}} = R_{\text{stent}} - R_0$ is the amount of overdilation. Note that the term “overdilation” refers here to any case where the stent radius is greater than the mean radius of the vessel before stenting R_0 . This is somewhat different from the clinical practice where the term “overdilation” corresponds to cases where the stent radius (after recoil) is greater than the maximum (systolic) radius of the vessel close to the prosthesis (although the difference between mean and maximum radius can hardly be measured routinely).

3.2. Numerical results

Several 2D axisymmetric simulations have been performed based on the computational domain and wall motion described in Section 3.1. In all cases, the bulk Reynolds number based on the steady part of the flow rate Q_0 and the mean radius R_0 is close to $R_b = 102$. The Womersley number is $W_0 = 3.36$. The velocity profile is imposed at the inlet section $x = x_{\text{inlet}}$ following the Womersley solution in elastic tubes and a zero constraint condition is used at the outlet section $x = x_{\text{outlet}}$. In order to assess the effect of the inlet/outlet boundary conditions on the results, computational domains with two different lengths have been considered. Two different spatial resolutions were also used in order to assess the spatial discretization errors. The

main characteristics of the calculations performed are given in Table 1 where Δx is the grid spacing in the streamwise direction in the area $x_1 < x < x_2$ and Δr refers to the grid spacing in the radial direction. Runs R1 and R2 correspond to reference calculations without endovascular prosthesis, the artery being fully rigid (no wall displacement) for R1 and elastic for R2. Labels R3(x) and R4 correspond to runs with stenting, the overdilation being non-zero only for the latter where $\delta R_{\text{stent}} = \varepsilon R_0$ (the stent radius is equal to the artery radius at systole). Recall that the term “overdilation” refers here to a stent whose radius is greater than R_0 (see Section 3.1). For all the cases considered in Table 1, the relative variation of the radius of the stented vessel $(\delta R(x, t) - R_0)/R_0$ is less than 5%, which is consistent with the linear elasticity assumption used to derive Eq. (3.1). When present, the stent is between $x_1 = 34 \text{ mm}$ and $x_2 = 47 \text{ mm}$. Runs whose label contains “a” have been performed with a longer computational domain than others. Labels containing letter “b” correspond to runs with finer mesh in the streamwise direction. In all cases, four cardiac cycles were first computed in order to reach a periodic state. A fifth cycle was then computed in order to analyse the results and compare the different physical/numerical configurations. Comparisons of the runs R2, R2a and R3, R3a, R3b (not shown) indicate that there is no significant effect of the numerics in the stent region (Nicoud, 2002). The differences observed between R1, R2, R3 and R4 are thus relevant to the stenting effects.

Time evolutions of the flow rate at inlet and outlet sections are displayed in Fig. 3 for case R2. The constraint that was introduced in Section 3.1 in order to set the speed of propagation of the pressure wave is fulfilled satisfactorily. Indeed, the flow rate at $x = x_{\text{outlet}}$ is the signal at $x = x_{\text{inlet}}$ with a time lag close to $(x_{\text{outlet}} - x_{\text{inlet}})/c \simeq 80/2492 \simeq 0.032 \text{ s}$. In the absence of endovascular prosthesis, all the physical quantities are self-similar with the constant speed of propagation c along the computational domain. Due to the wall displacement, Eq. (3.1), the WSS is not uniform over the streamwise direction, as depicted in Fig. 4 at four different instants. Instead it is alternatively increasing and decreasing along the domain depending on the phase considered. In the case where the vessel is not compliant, there should be no time lag between shear stress signals at different locations since the exact Womersley profile is imposed at $x = x_{\text{inlet}}$. Accordingly, the WSS is mostly uniform (not exactly uniform because of small side effects due to the inlet/outlet boundary conditions) over the streamwise distance in the case R1 (see Fig. 4).

The shape of the computational domain for cases R2, R3 and R4 is shown in Fig. 5 for times $t = nT$ (corresponding to systole at the inlet section) and $t = (n + 1/2)T$ (diastole). The non-compliant region which

Table 1
List of the axisymmetric calculations performed with their main numerical characteristics

Run	Wall motion	ε	δR_{stent}	x_{inlet}	x_{outlet}	Δx	Δr	# of grid points
R1	$R(x, t) = R_0$	0.0	No stent	0	80	0.075	0.286	3528
R2	Eq. (3.1)	0.05	No stent	0	80	0.075	0.286	3528
R3	Eq. (3.3)	0.05	0.0	0	80	0.075	0.286	3528
R4	Eq. (3.3)	0.05	0.075	0	80	0.075	0.286	3528
R2a	Eq. (3.1)	0.05	No stent	-30	110	0.075	0.286	4368
R3a	Eq. (3.3)	0.05	0.0	-30	110	0.075	0.286	4368
R3b	Eq. (3.3)	0.05	0.0	0	80	0.050	0.286	5208

Lengths and axial positions are in millimetres.

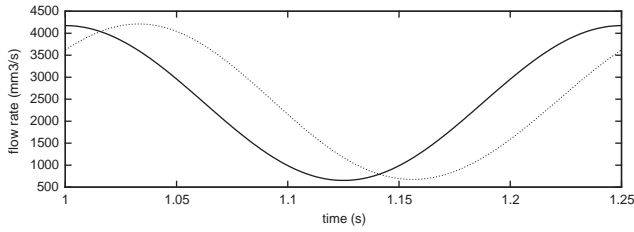


Fig. 3. Time evolutions of the flow rate at sections —: $x = x_{\text{inlet}}$ and: $x = x_{\text{outlet}}$ for the case R2. Note that the origin of time is 1 s since the fifth cycle is analysed (see text).

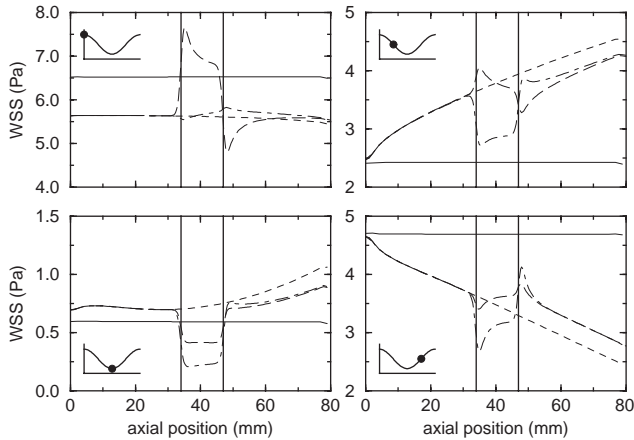


Fig. 4. WSS for runs R1 (solid), R2 (dashed), R3 (long dashed) and R4 (dot-dashed) at times: $t = nT$ (systole: top left), $t = (n + 1/4)T$ (top right), $t = (n + 1/2)T$ (diastole: bottom left) and $t = (n + 3/4)T$ (bottom right), where $T = 2\pi/\omega$ is the period. The two vertical lines denote the stent location.

mimics the endovascular prosthesis is clearly visible (cases R3 and R4) in the central region. The isolines of the streamwise velocity show that the flow accelerates when the cross-section area decreases. The effect of the wall motion mismatch on the WSS is also shown in Fig. 4. At systole, this quantity is larger in the medium part of the stented region ($x \simeq 40$ mm) than in the non-stented artery when the stent is not overdilated. This is consistent with the fact that the cross-section area in R3

and at systole is smaller in the prosthesis zone (see Fig. 5). On the contrary, when the stent is slightly overdilated, the WSS at systole is not drastically modified by the prosthesis. Indeed, stenting does not induce any geometrical perturbation in this case (see Figs. 4 and 5, case R4). At diastole, the cross-section area at the stent level is larger and the WSS is smaller. Comparing the cases R3 and R4, we note that this effect is amplified by a slight increase of the stent diameter. However, the impact of the stent overdilation on the WSS modification is not as pronounced at diastole than during systole.

4. Discussion

Let us first consider the analytical result derived in Section 2. A typical value of the speed of propagation of waves in (human coronary) arteries being a few meters per second, the wavelength is usually a few meters. On the other hand, the length scale of the stent is most likely equal to a few centimetres, meaning that the module of the dimensionless parameter $k_2 L_2$ in Eq. (2.4) is small compared to unity. Moreover, since the goal of this study is to assess the wave reflection specific the endovascular prosthesis, one can assume that zero reflection occurs in absence of stent, viz. $A_1 K_1 = A_3 K_3$ (in other words, we assume that host artery is perfectly homogeneous). Finally, expanding Eq. (2.4) as a power series of the parameter $k_2 L_2$, one obtains the following first-order expression for the reflection coefficient:

$$R_{\text{stent}} = \frac{j(1 - A^2)}{2A} k_2 L_2 + O(k_2^2 L_2^2), \quad A = \frac{A_1 K_1}{A_2 K_2}. \quad (4.1)$$

This relation shows that the theoretical reflection induced by an endovascular prosthesis increases with both the pulsation of the wave and the length of the stent. Moreover, it is zero as soon as $A = 1$, viz. $A_1 K_1 = A_2 K_2$. Assuming that viscous and viscoelastic effects can be neglected in the reflection process makes A and k_2 real numbers with $A = \sqrt{A_1 A'_1 / A_2 A'_2}$ and $k_2 L_2 = \omega \sqrt{\rho A'_2 / A_2 L_2}$. Eq. (4.1) then leads to a convenient

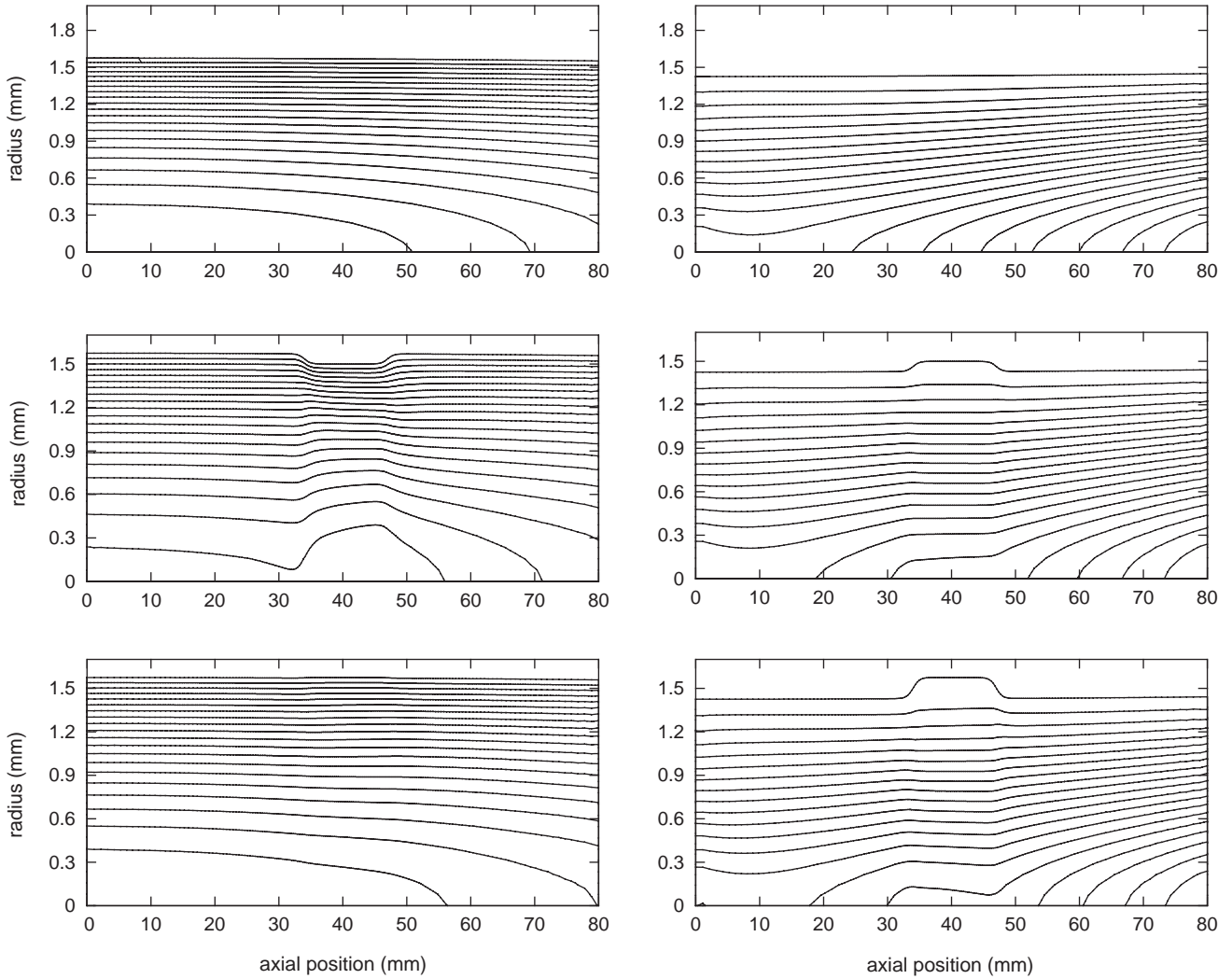


Fig. 5. Shape of the computational domain at times $t = nT$ (systole: left column) and $t = (n + 1/2)T$ (diastole: right column) for the runs R2 (top row), R3 (middle row) and R4 (bottom row). The isolines of the streamwise velocity are plotted. The streamwise and radial coordinates are expressed in millimetres. The aspect ratio R_0/L has been multiplied by 35 for convenience.

formula to assess the amount of wave reflection:

$$R_{\text{stent}} \simeq j\omega\sqrt{\rho} \frac{A_2 A'_2 - A_1 A'_1}{2\sqrt{A_1 A'_1}} \frac{L_2}{A_2}. \tag{4.2}$$

From this relation, the amount of wave reflection is related to the geometrical/mechanical mismatch induced by the stenting, a stent shape factor L_2/A_2 as well as the flow conditions. This is coherent with the findings of Formaggia et al. (2001) who numerically solved the 1D non-linear flow equations in a distensible pipe with spatially variable compliance. Since they did not consider harmonic signals, it is difficult to deduce frequency-dependent reflection coefficients from their simulations and compare their numerical results with Eq. (4.2). However, in agreement with the present model, they clearly established that the amount of reflection increases with the stent shape factor and

compliance mismatch. Finally, Eq. (4.2) shows that a stent satisfying the relation $A_2 = A_1 A'_1/A'_2$ produces no wave reflection. Clearly, such a prosthesis is not realistic since experimental measurements have shown that A'_1/A'_2 is as high as 5 (see Section 3.1). However, since the compliance A'_2 of the stented artery is always smaller than the compliance A'_1 of the host artery, it follows from Eq. (4.2) that overdilation ($A_2 > A_1$) tends to reduce the amount of reflected waves.

Regarding the numerical results of Section 3, recall that the objective of the study is to assess the response of blood motion to geometrical perturbations induced by the compliance mismatch (itself induced by the presence of the prosthesis). To address this issue, it is relevant to consider the wall motion as an input and to look at modifications in blood flow when stenting is accounting for in the design of this input. Indeed, this approach provides valuable information regarding the

haemodynamic changes due to stenting while avoiding to solve the coupled, computer time consuming fluid–structure interaction problem. Still, the design of the input wall motion must be consistent with the effective geometrical changes observed experimentally. Eq. (3.3) has been used in this numerical study to model the wall displacement of an elastic stented artery. It is coherent with the animal experiments (Vernhet et al., 2001) with respect to at least three important aspects of the endovascular stenting:

- it assumes that the speed of propagation within the prosthesis is infinite which is consistent with the fact that the measured compliance at the stent level is several times smaller than its value before/after stenting,
- using the approximation Eq. (4.2) and the numerical values provided in Section 3.1, the modulus of the reflection coefficient under in vivo conditions is approximately $|R_{\text{stent}}| \simeq 2\%$. It is never more than a few percents if one considers the most unfavourable experimental values in Vernhet et al. (2001). As a result, the pressure field is mostly related to the forward pressure wave, which justifies the fact that no back propagating wave is accounted for in Eq. (3.3).
- although we do not claim that the hyperbolic tangent is the “exact” functional form of the buffer region between the elastic artery and the stent, it is a reasonable candidate for modelling the transition zone. Moreover, the analytical transition length is of order 3 mm (this is a direct consequence of the damping function $f(x)$). This value is in agreement with the observations made during the animal experimentations and showing that the buffer region is close to one diameter long.

Table 2 shows the values of the WSS at the middle of the stent, viz. $x = (x_1 + x_2)/2 \simeq 40$ mm. The amplitude of this quantity over the cardiac cycle is larger for the stented vessel than it is for the elastic artery. It is worth noting that although the length of the stent is very small as compared to the wavelength, the WSS amplitude in case R3 behaves more like in case R1 (fully rigid tube) and less like in case R2 (elastic tube). The slight overdilation of the prosthesis, by avoiding the increase in shear stress at systole (there is no geometry discontinuity at systole for the case R4, see Fig. 5), limits drastically the increase in stress amplitude. Fig. 4 in Section 3.2 suggests that the most important flow changes do not appear near the middle of the stent. This is indeed confirmed by Fig. 6 where the amplitude of WSS variations over the cycle for cases R3 and R4 is plotted as functions of the axial position. Since these quantities are scaled by their value for the non-stented vessel (case R2), this figure offers a measure of the haemodynamic changes due to the prosthesis in cases

R3 and R4. Note that near the stent middle, the values reported in Table 2 are recovered. The maximal changes are located slightly downstream the ends of the stent. Near the proximal edge, the WSS variation over the cardiac cycle increases by 50% in amplitude whereas it decreases by roughly 20% downstream the distal end of the prosthesis. The modulus of the spatial gradient of the WSS fluctuations is also drastically increased in both edge regions. These findings might be related to the clinical observation that there is a first-order edge effect in some type of restenosis where intimal hyperplasia mostly develops near the stent ends (Weissman et al., 2001). Finally, Fig. 6 suggests that a slight increase in the stent diameter may reduce drastically the WSS changes induced by stenting. Noticeably, the modifications near the transition regions for the case R4 are smaller than inside the stent.

This theoretical/numerical study supports the idea that stenting can induce endothelial dysfunction via haemodynamic perturbations. Although the amount of pressure reflection is most likely negligible due to the small stent-to-wavelength ratio, the amplitude of the WSS variation over the cardiac cycle is alternatively increased (by 35% at the middle of the stent, by 50% in the proximal transition region) and decreased (by 20% in the distal transition region) by long-standing stenting. Note that the later findings are in good agreement with recent results of Tortoriello and Pedrizzetti (2004). These authors, by using a perturbative method to solve the fluid–tissue coupled problem numerically, have shown that stenting decreases the diastolic WSS. They attributed this result to the fact that, during diastole, the artery shrinks more than the stiffer stented region, which is consistent with Fig. 5. They also found that the maximum changes were located near the edges of the stent. However, in contrast to Fig. 4, they did not observe a large increase of systolic WSS. This seems to be a direct consequence of the geometrical bump that their stented artery experiences during systole at the prosthesis edges. This local deformation, which is related to the particular spatial variations of vessel radius and compliance that have been used by Tortoriello and Pedrizzetti (2004), is not present in our study.

Our results suggest also that over-dilated stents produce less haemodynamic perturbations: (1) From the pressure wave point of view, overdilation tends to lower the amount of reflection, the optimal overdilation being proportional to the compliance ratio. With the typical amount of compliance mismatch observed after stenting (see Section 3.1), this result leads to an “optimal” over-expansion close to 600%. Of course this value is unrealistic for clinical applications. It reflects the fact that only acoustic has been accounted for in the 1D model of Section 2 and that stenting does not modify the pressure wave propagation drastically: recall that the reflection coefficient is only a few percents

Table 2

Minimum, maximum and (scaled) variations of the WSS for different runs at the middle of the stent

Run	min(WSS)	max(WSS)	Δ WSS	Δ WSS/ Δ WSS _{runR2}
R1	0.39	6.72	6.33	1.29
R2	0.72	5.62	4.90	1.00
R3	0.42	6.98	6.56	1.34
R4	0.22	5.66	5.44	1.11

Stresses are in Pa.

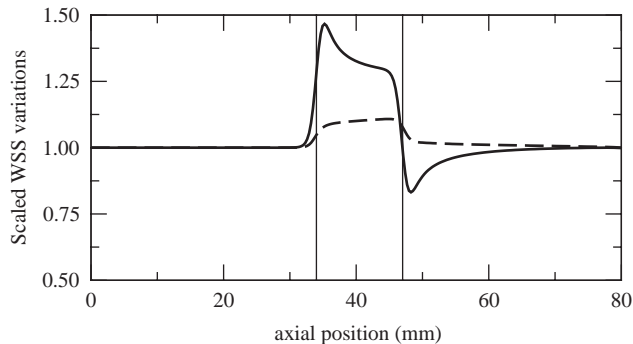


Fig. 6. Scaled amplitude of the WSS fluctuations for runs R3 (solid) and R4 (long-dashed) The two vertical lines denote the stent location.

because the stent-to-wavelength ratio is always small in clinical applications. (2) The increase of the systo-diastolic WSS fluctuations is only 10% when the stent radius matches the artery one at systole. Under in vivo conditions, the efficiency of stenting does not depend only on haemodynamics and other effects must be accounted for. Regarding stent over-dilation, an increased intimal hyperplasia is always demonstrated (Vernhet et al., 2003; Schwartz et al., 1992) despite contradictory clinical consequences (Caixeta et al., 2000; Koyama et al., 2000) are reported in the literature. However, it is likely that an optimum over-dilation rate exists, which limits the amount of haemodynamic perturbations without inducing unacceptable vascular stretching. Further studies are necessary to clarify this issue.

5. Conclusion

Two simple models have been developed and used in order to study the changes in blood motion due to long-standing stenting. The details of the stent structure were not accounted for because the objective was to focus on the mid-term (after the wires have been integrated with the surrounding tissue) effects of stenting on haemodynamics. Accordingly, the prosthesis was modelled as a uniform rigid tube embedded in an elastic artery and the effects of the compliance mismatch have been studied.

The first model is fully analytical and allow to assess the amount of pressure wave reflection due to stenting under the 1D assumption. An easy-to-use formula is provided in order to assess the reflection coefficient from the knowledge of the compliance before and after stenting. It is found that it is proportional to the stent-to-wavelength ratio and that the amount of wave reflection remains rather small in clinical applications. This result is the basis of the second numerical model developed in order to assess the wall shear stress changes. In this approach, the fully coupled fluid–structure problem is replaced by a simpler fluid problem with moving boundaries. The amount of pressure reflection being small, a simple analytical law can be used to describe the wall motion over space and time. The Navier–Stokes equations are then solved numerically with an appropriate finite-element-based method which handles time-dependent geometries. The main result is that, due to stenting and the corresponding compliance mismatch, the amplitude of the wall shear stress variations is drastically increased, by more than 30% at the middle of the stent, more than 50% in the proximal transition region. These results support the idea that stenting can induce endothelial dysfunction via haemodynamic perturbations. They are also consistent with the fact that intimal hyperplasia is often more developed near the edges of the stents. Finally, our numerical simulations indicate that the negative effects of long-standing stenting on haemodynamics decrease when the radius of the prosthesis is slightly increased.

References

- Bénard, N., Coisne, D., Perrault, R., 2003. Simulation of blood flow in stented artery: blood rheological properties effects. In: XXVIII Congrès, Poitiers, France. Société de Biomécanique.
- Berry, J., Santamarina, A., Moore, J., Roychowdhury, S., Routh, W., 2000. Experimental and computational flow evaluation of coronary stents. *Annals of Biomedical Engineering* 28, 386–398.
- Caixeta, A., Brito, F.J., Rati, M., 2000. High versus low-pressure balloon inflation during multilinktrade mark stent implantation: acute and long-term angiographic results. *Catheter and Cardiovascular Interventions* 50, 398–401.
- Caro, C., Fitz-Gerald, J., Schroter, R., 1969. Arterial wall shear and distribution of early atheroma in man. *Nature* 211 (223), 1159–1160.
- Chorin, J., 1967. A numerical method for solving incompressible viscous flow problems. *Journal of Computational Physics* 2, 12–26.
- Davies, P., Shi, C., DePaola, N., Helmke, B., Polacek, D., 2001. Hemodynamics and the focal origin of atherosclerosis. a spatial approach to endothelial structure, gene expression, and function. *Annals of The New York Academy of Sciences* 947, 7–16.
- Formaggia, L., Nobile, F., Quarteroni, A., 2001. A one dimensional model for blood flow: application to vascular prosthesis. In: Miyoshi, T. (Ed.), In MSCOM2000. Springer, Berlin.
- Grube, E., Silber, S., Hauptmann, K., Mueller, R., Buellfeld, L., Gerckens, U., Russell, M., 2003. Taxus i: six- and twelve-month results from a randomized, double-blind trial on a slow-release paclitaxel-eluting stent for de novo coronary lesions. *Circulation* 107 (1), 38–42.

- Hughes, T., Lubliner, J., 1973. On the 1D theory of blood flow in the larger vessels. *Mathematical Biosciences* 18, 161–170.
- Koyama, J., Owa, M., Sakurai, S., 2000. Relation between vascular morphologic changes during stent implantation and the magnitude of in-stent neointimal hyperplasia. *American Journal of Cardiology* 86, 753–758.
- Medic, G., Mohammadi, B., 1999. Nsike—an incompressible Navier–Stokes solver for unstructured meshes. INRIA Research Report 3644.
- Morice, M., Serruys, P., Sousa, J., Fajadet, J., Ban Hayashi, E., Perin, M., Colombo, A., Schuler, G., Barragan, P., Guagliumi, G., Molnar, F., Falotico, R., 2002. Ravel study group. Randomized study with the sirolimus-coated bx velocity balloon-expandable stent in the treatment of patients with de novo native coronary artery lesions. A randomized comparison of a sirolimus-eluting stent with a standard stent for coronary revascularization. *New England Journal of Medicine* 346 (23), 1773–1780.
- Nicoud, F., 2002. Hemodynamic changes induced by stenting in elastic arteries. Center for Turbulence Research, CTR Annual Research Briefs, pp. 336–347.
- Rau, T., Schofer, J., Schluter, M., Seidensticker, A., Berger, J., Mathey, D., 1998. Stenting of non acute total coronary occlusions: predictors of late angiographic outcome. *Journal of American College of Cardiology* 31, 275–280.
- Reuderink, P., Hoogstraten, H., Sipkema, P., Hillen, B., Westerhof, N., 1989. Linear and nonlinear one-dimensional models of pulse wave transmission at high womersley numbers. *Journal of Biomechanics* 22, 819–827.
- Robinson, K., Roubin, G., Siegel, R., Black, A., Apkarian, R., King, S., 1988. Intra-arterial stenting in the atherosclerotic rabbit. *Circulation* 78, 646–653.
- Rolland, P., Charifi, A., Verrier, C., 1999. Hemodynamics and wall mechanics after stent placement in swine illiac arteries: comparative results from six stent designs. *Radiology* 213, 229–246.
- Schwartz, R., Huber, K., Murphy, J., 1992. Restenosis and the proportional neointimal response to coronary artery injury: results in a porcine model. *Journal of American College of Cardiology* 19, 267–274.
- Serruys, P., Degertekin, M., Tanabe, K., Abizaid, A., Souza, J., Colombo, A., Guagliumi, G., Wijns, W., Lindeboom, W., Ligthart, J., de Feyter, P., Morice, M., 2002. Intravascular ultrasound findings in the multicenter, randomised double-blind ravel (randomised study with the sirolimus-eluting velocity balloon-expandable stent in the treatment of patients with de novo native coronary artery lesions) trial. *Circulation* 106, 798–803.
- Tortoriello, A., Pedrizzetti, G., 2004. Flow-tissue interaction with compliance mismatch in a model stented artery. *Journal of Biomechanics* 37, 1–11.
- Vernhet, H., Juan, J., Demaria, R., Oliva-Lauraire, M., Sénac, J., Dauzat, M., 2000. Acute changes in aortic wall mechanical properties after stent placement in rabbits. *Journal of Vascular and Interventional Radiology* 11 (5), 634–638.
- Vernhet, H., Demaria, R., Oliva-Lauraire, M., Juan, J., Sénac, J., Dauzat, M., 2001. Changes in wall mechanics after endovascular stenting in rabbit aorta: comparison of three different stent designs. *American Journal of Roentgenology* 176 (3), 803–807.
- Vernhet, H., Demaria, R., Pérez-Martin, A., Juan, J., Oliva-Lauraire, M., Marty-Double, C., Sénac, J., Dauzat, M., 2003. Wall mechanics of the stented rabbit aorta: long-term study and correlation with histological findings. *Journal of Endovascular Therapy* 10 (3), 577–584.
- Weissman, N., Wilensky, R., Tanguay, J., Bartorelli, A., Moses, J., Williams, D., Bayley, S., Martin, J., Canos, M., Rudra, H., Popma, J., Leom, M., Kaplan, A., Mintz, G., 2001. Extent and distribution of in-stent intimal hyperplasia and edge effect in a non-radiation stent population. *American Journal of Cardiology* 88, 248–252.
- Womersley, J., 1955. Oscillatory motion of a viscous liquid in a thin-walled elastic tube- i: the linear approximation for long waves. *Philosophical Magazine (series 7)* 46, 199–221.